On the dosimetric behaviour of photon dose calculation algorithms in the presence of simple geometric heterogeneities: comparison with Monte Carlo calculations

2007 Phys. Med. Biol. 52 1363

(http://iopscience.iop.org/0031-9155/52/5/011)

IOP Publishing Physics in Medicine and Biology

Phys. Med. Biol. **52** (2007) 1363–1385 doi:10.1088/0031-9155/52/5/011

On the dosimetric behaviour of photon dose calculation algorithms in the presence of simple geometric heterogeneities: comparison with Monte Carlo calculations

Antonella Fogliata[1], Eugenio Vanetti[1,2], Dirk Albers[4], Carsten Brink[5], Alessandro Clivio[1,2], Tommy Knöös[3], Giorgia Nicolini[1] and Luca Cozzi[1]

[1] Oncology Institute of Southern Switzerland, Medical Physics Unit, Bellinzona, Switzerland
[2] Medical Physics Specialisation School, University of Milan, Italy
[3] Radiation Physics, Lund University Hospital, Sweden
[4] Department of Radiotherapy and Radio-Oncology, University Medical Center Hamburg-Eppendorf, Germany
[5] Laboratory of Radiation Physics, Odense University Hospital, Denmark

E-mail: lucozzi@iosi.ch

Received 19 July 2006, in final form 2 January 2007
Published 8 February 2007
Online at stacks.iop.org/PMB/52/1363

Abstract

A comparative study was performed to reveal differences and relative figures of merit of seven different calculation algorithms for photon beams when applied to inhomogeneous media. The following algorithms were investigated: Varian Eclipse: the anisotropic analytical algorithm, and the pencil beam with modified Batho correction; Nucletron Helax-TMS: the collapsed cone and the pencil beam with equivalent path length correction; CMS XiO: the multigrid superposition and the fast Fourier transform convolution; Philips Pinnacle: the collapsed cone. Monte Carlo simulations (MC) performed with the EGSnrc codes BEAMnrc and DOSxyznrc from NRCC in Ottawa were used as a benchmark. The study was carried out in simple geometrical water phantoms ($\rho = 1.00$ g cm^{-3}) with inserts of different densities simulating light lung tissue ($\rho = 0.035$ g cm^{-3}), normal lung ($\rho = 0.20$ g cm^{-3}) and cortical bone tissue ($\rho = 1.80$ g cm^{-3}). Experiments were performed for low- and high-energy photon beams (6 and 15 MV) and for square (13×13 cm^2) and elongated rectangular (2.8×13 cm^2) fields. Analysis was carried out on the basis of depth dose curves and transverse profiles at several depths. Assuming the MC data as reference, γ index analysis was carried out distinguishing between regions inside the non-water inserts or inside the uniform water. For this study, a distance to agreement was set to 3 mm while the dose difference varied from 2% to 10%. In general all algorithms based on pencil-beam convolutions showed a systematic deficiency in managing the presence of heterogeneous media. In contrast, complicated patterns were observed for the advanced algorithms

with significant discrepancies observed between algorithms in the lighter materials ($\rho = 0.035$ g cm^{-3}), enhanced for the most energetic beam. For denser, and more clinical, densities a better agreement among the sophisticated algorithms with respect to MC was observed.

S This article has associated online supplementary data files

(Some figures in this article are in colour only in the electronic version)

1. Introduction

Verification of the accuracy in dose calculation is an important task in the entire chain of the radiotherapy process and related quality assurance procedures. On the subject, there are several documents at international level, as the technical report by IAEA (IAEA TRS-430 2005) where it is recommended to divide the verifications into benchmark, generic beam and user's beam data verifications. Other documents are e.g. the IEC62083 (2000), or, from other communities, the AAPM Report 85 (2004) and the ESTRO booklet no 7 (Mijnheer *et al* 2004).

The aim of the present study was to investigate the performances and to quantify the relative differences of a group of algorithms for photon dose calculation for external radiotherapy treatment planning systems (TPS). All the included TPS were commercially available and released for clinical usage. The study was limited to explore the ability of different algorithms to manage the presence of materials different from water when computing three-dimensional dose distributions. This aim was translated into a set of computational experiments performed on simple geometrical phantoms. Monte Carlo simulations (MC) were performed and used as a reference benchmark to validate the calculations performed by TPS. Similar studies have appeared in recent years but mostly limited to one or two algorithms using either MC or measurements as a benchmark.

For example the multigrid superposition and the fast Fourier convolution implemented by CMS in the Focus TPS (precursor of the recent XiO which was included in this study) have been validated against measurement with radiographic films and ion chambers (Garcia-Vicente *et al* 2003). Comparisons with the multigrid superposition against MC simulations in phantoms with different densities (lung and bone) have also been published (Miften *et al* 2001). Both publications reported agreements between TPS and validation data better than 3% and 3 mm.

Concerning collapsed cone, as implemented in the Helax-TMS system, it has extensively been tested by several groups in various geometries against MC (Aspradakis *et al* 2003, Carrasco *et al* 2004, Nisbet *et al* 2004, Paelinck *et al* 2005, Weber and Nilsson 2002). In the simpler cases measurements were also included, e.g. Aspradakis *et al* performed measurements either in water (with ion chambers) or inside lung equivalent materials (with films). Carrasco *et al* compared depth doses with TLDs and Nisbet *et al* used either TLDs or ion chambers in simple slab phantoms or in the Rando Alderson phantom. The Paelinck *et al* study used Gafcromic films for verifications and in the paper by Weber and Nilsson measurements were performed with ion chambers and diodes in uniform water geometries. Results, with a variety of different 'acceptance criteria' are all consistently positive even in the presence of particular cases where additional investigations would be necessary.

Another study performed by Jones and Das (2005) compared MC and the collapsed cone implementation in Pinnacle. This paper confirmed the good results expected from the collapsed

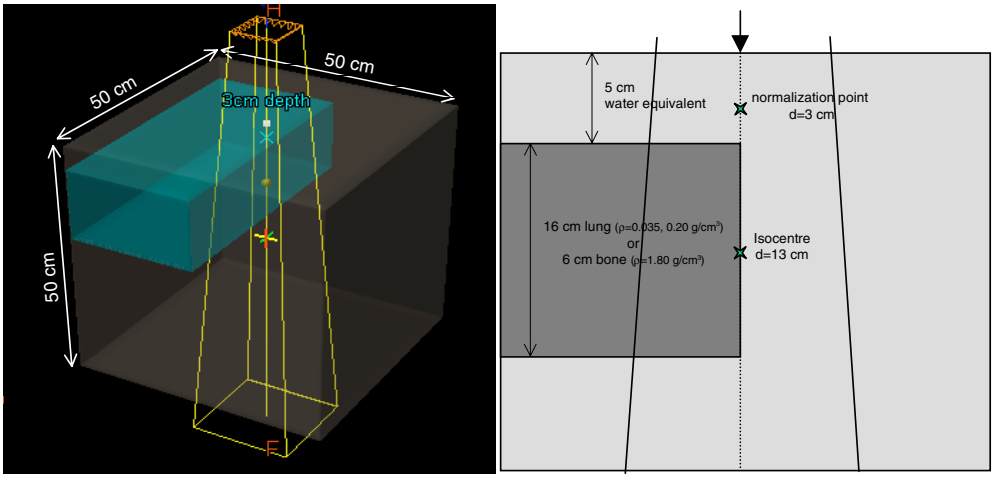

Figure 1. Geometrical layout of the phantom.

cone in simple geometries including the lung, which have been proved earlier regarding the Helax-TMS collapsed cone implementation.

Even if some of the experiments and results of the studies mentioned above will be partly replicated and thus confirmed by the data presented here, this study offers the possibility of comparing simultaneously the performance of several models under identical conditions. It will also allow the establishment of a basic evaluation tool for the most popular planning algorithms used in clinical practice today.

More sophisticated studies in anthropomorphic phantoms and in patients are scheduled and will be performed in a second stage as part of a larger research project. An independent study has been already published (Knöös *et al* 2006) comparing the qualitative performance of these algorithms on a group of clinical cases against MC simulations.

2. Materials and methods

2.1. The heterogeneous phantom

To perform all calculations, a virtual phantom was defined and stored in appropriate DICOM and DICOM-RT objects (pseudo-CT slices and volumes) and distributed to all participants. The phantom was set up to have two constituents: water ($\rho = 1.00$ g cm^{-3}) and a second material. Three groups of experiments were carried out with the second material: (a) light lung: $\rho = 0.035$ g cm^{-3} (b) normal lung: $\rho = 0.20$ g cm^{-3}, (c) bone: $\rho = 1.80$ g cm^{-3}. All materials were defined as water with different mass density. It has to be noticed that the 'light' and 'normal' terms used for (a) and (b) shall be read in relative terms. The 'light lung' case represents a sort of extreme inferior limit of applicability of the algorithms and corresponds to density found in human bodies only in small amounts (similar to, e.g., air cavities as trachea, where the density is not fully as free air). The lung density used in the literature ranges from 0.2 to 0.35 g cm^{-3} while for cortical bone (bone in the following) it ranges from 1.80 to 2.04 g cm^{-3} (e.g. Carrasco *et al* (2004), Miften *et al* (2001), Nisbet *et al* (2004)). Figure 1 shows schematically how the phantom was defined.

The size of the phantom was $50 \times 50 \times 50$ cm^3. Water was used in the first 5 cm of depth, d. The layer between $d = 5$ and $d = 21$ cm was divided into two regions (separated by

the central axis) as depicted in figure 1: water was defined on one side while the other side was defined with a different density to simulate the presence of a heterogeneity. For the bone experiments, this layer was reduced in thickness from 16 cm to 6 cm ending instead at $d = 11$ cm. Water was defined again after the distal edge of the insert, i.e. from $d = 21$ cm (11 cm in the bone case) down to $d = 50$ cm.

2.2. The algorithms under investigation and the Monte Carlo reference

Seven different algorithms released for clinical application from four commercial TPS were included in the study.

(1) Varian Eclipse TPS:
- anisotropic analytical algorithm (AAA-ECL), release 7.5.14.3;
- single pencil-beam convolution (PBC-ECL) with the modified Batho correction, release 7.5.14.3.

(2) Nucletron Helax-TMS TPS:
- collapsed cone (CC-TMS), release 6.1A;
- pencil-beam convolution (PB-TMS), with the equivalent path length correction, release 6.1A.

(3) Philips Pinnacle TPS:
- collapsed cone (CC-PIN), release 7.6c.

(4) CMS XiO TPS:
- multigrid superposition/convolution (MGS-XiO), release 4.2.0;
- fast Fourier transform convolution (FFTC-XiO), release 4.2.0.

These algorithms can be classified into two groups.

(i) Models primarily based on equivalent path length (EPL) for inhomogeneity corrections, where electron transport is not separately modelled, and the density changes are sampled along the 1D primary rays. The two pencil-beam algorithms PBC-ECL and PB-TMS, and the fast Fourier convolution algorithm FFTC-XiO belongs to this group which in the following will be referred to as 'type-a' algorithms.

(ii) Models able to treat the electron transport in an approximate way as well as the secondary photon transport in the medium accounting for density changes, sampled along the full three dimensions. The two collapsed cone algorithms CC-TMS and CC-PIN, the AAA-ECL and the MGS-XiO belong to this group of 'advanced' models defined in the following as 'type-b' algorithms.

Readers are referred to the original publications since a detailed description of the algorithms is beyond the aims and the space limits of this publication. In the appendix, a brief description of the analysed algorithms is reported while a more detailed discussion can also be found in Knöös *et al* (2006).

For the Monte Carlo simulations, all calculations have been performed with EGSnrc as the engine for the BEAMnrc and DOSXYZnrc user codes from the NRCC group (Rogers *et al* 1995, Kawrakow 2000a, 2000b, Kawrakow *et al* 2004). A virtual linac was simulated with a source emitting photons sampled from spectral distributions producing depth doses and lateral distributions with the required penetration. Photons are transported through an ideal collimator with no transmission or scatter production (Wieslander and Knöös 2000). During the phantom simulations with DOSXYZnrc, 75 million particles were used per field to yield a maximum

Table 1. Beam qualities (expressed as $TPR_{20/10}$) for the 6 and 15 MV photon beams used for all dose calculation algorithms and MC simulations. TPR are as computed by the corresponding systems. The error reported in the mean value is at one standard deviation.

Algorithm	$TPR_{20/10}$ (6 MV)	$TPR_{20/10}$ (15 MV)
AAA-ECL	0.673	0.760
PBC-ECL	0.670	0.764
CC-TMS	0.684	0.762
PB-TMS	0.672	0.763
CC-PIN	0.667	0.759
FFTC-XiO	0.675	0.763
MGS-XiO	0.674	0.762
MC	0.675	0.752
Mean	0.674 ± 0.005	0.761 ± 0.004

statistical uncertainty of around 2%. The resolution of the three-dimensional phantom was 0.25 cm in all three directions. The selected transport parameters were set according to the default settings of the code system except the total energy cut-off for electrons and photons: ECUT was 700 keV, and the PCUT was 10 keV.

2.3. Investigated beams and analysis tools

Two photon beam energies of 6 and 15 MV were selected for the study. Ideally the same set of commissioning measurements (i.e. algorithm input data) should be implemented in each TPS. This was pragmatically impossible since each TPS requires substantially different sets of input data and no set, extensive enough for the purpose, was available. It was therefore decided to use beam data already implemented in the different systems provided that consistency in beam quality and shapes of reference depth dose and profiles were granted. This approach was also used in a previous study (Knöös *et al* 2006). Table 1 summarizes, for all the algorithms, the corresponding qualities ($TPR_{20/10}$) of the beams used for the calculations.

Similarly, to produce Monte Carlo simulations, all the accelerators and beams used for the experiments should be modelled. This was, however, not realistically achievable and therefore a simplified linear accelerator was used as described by Wieslander and Knöös (2000, 2003).

For each individual beam energy and calculation algorithm used in this study, a validation test was, as anticipated, performed by comparing depth dose curves and profiles at 5 and 10 cm depth for $10 \times 10\ cm^2$ and $20 \times 20\ cm^2$ field sizes in homogeneous water phantoms against the corresponding Monte Carlo simulations. Ion chamber measurements, performed on a Varian Clinac 2100 C/D for both energies, were added in the comparison to strengthen the validation.

For all three groups of experiments (light lung, normal lung and bone), dose distributions generated by two field sizes per energy were computed and analysed, a square field of $13 \times 13\ cm^2$ and a narrow rectangular field of $2.8 \times 13\ cm^2$. For the latter, the long axis was crossing the heterogeneity boundary. In total, 12 experiments were carried out (2× energy, 2× field size, 3× heterogeneity). The central beam axis (i.e. the collimator axis) was always positioned along the heterogeneity boundary. The isocentre was positioned at 13 cm depth (SSD = 87 cm) as shown in figure 1. Gantry and collimator angles were set to 0° (a further study will be devoted to appraise different incidences). All scales follow the IEC 1217 convention.

For each experiment, depth dose curves (DD) and transverse profiles across the heterogeneity were analysed. Four DD were analysed (from $d = 0$ to $d = 30$ cm) at ±4 cm and at ±0.8 cm off-axis but parallel to the collimator axis.

Thirteen profiles were analysed at depths $d = 1, 2, 3, 6, 7, 9, 11, 13, 17, 19, 22, 23$ and 25 cm, partly in water and partly through the inserted non-water material. Calculation of dose profiles was extended at least 4 cm beyond the field edges at each depth.

The analysis was carried out for relative dose distributions. All data were normalized with a procedure similar to that described in Knöös *et al* (2006) and consistent to that suggested by ESTRO (Mijnheer *et al* 2004). For every algorithm and every energy and field, the number of monitor units (MU) and the dose D at 3 cm depth on the central beam axis were recorded in the presence of heterogeneity. A reference calculation (D_{ref}) was performed also for the same beam conditions, but without the heterogeneity present, recording the corresponding monitor units ($\mathrm{MU}_{\mathrm{ref}}$). Data were thus scaled according to the factor $(D/\mathrm{MU})/(D_{\mathrm{ref}}/\mathrm{MU}_{\mathrm{ref}})$. In this way, differences from monitor unit calculations, head scatter or phantom scatter modelling and simplified MC modelling were removed or at least their influence were minimized. For the MC data, normalization was performed as the ratio of the absolute dose per impinging photon in the test and reference conditions. In order to decrease the noise present in the MC data, the numerical values used for normalization were given by the average of the pixel content in an area of 0.75×0.75 cm^2 in a plane perpendicular to the beam axis at the proper depth.

To appraise quantitatively the discrepancies observed between TPS calculations and Monte Carlo simulations, an elliptical γ index analysis (Low *et al* 1998) was performed setting the MC data as reference. Distance to agreement (DTA) was set to 3 mm for all calculations. Different thresholds were used for the difference in dose (ΔD) from 2% to 10% (of the local MC dose) to investigate sensitivity to different dose thresholds. The analysis was performed for each profile at all available depths.

Dose calculations in Eclipse were performed using a grid size of 0.25 cm while export was at 0.025 cm (export resolution built into the system). In the Helax-TMS, calculations and exports were performed on a grid size of 0.1 cm. In both XiO and Pinnacle, calculations were performed with a grid size of 0.2 cm; data exported from XiO had a spatial resolution of 0.1 cm, from Pinnacle of 0.2 cm. All Monte Carlo simulations were performed with a scoring grid size of 0.25 cm. No smoothing nor data reduction were applied to either the depth dose or the profile data; for display and DD and profile analysis, an interpolation process was applied to TPS data to generate, if necessary, the same grid as for MC data. To compute the γ index, a resolution of 0.05 cm was applied to the TPS interpolating raw data if necessary.

In most TPS calculations only the relative electron density is considered, neglecting the mass composition while for CC-based systems a mapping to a medium is also performed, and calculations are done with dose to tissue. It has been proven in several publications that this effect is relatively small in lighter tissues like the lung while it is not negligible for the bone case (Siebers *et al* 2000, Dogan *et al* 2006, Knöös *et al* 2006). The elemental composition of bone differs substantially from water and all other water-like tissues present in the body. For that reason MC simulations were performed and reported in terms of dose to water rather than dose to media for the two lung cases while for bone, two sets of MC simulations were performed: one ($\mathrm{bone}_{\mathrm{w}}$) assuming water as material and scaling only the density and a second ($\mathrm{bone}_{\mathrm{t}}$) using cortical bone as tissue with the proper composition (ICRU 1989) and computing dose delivered to that medium. In the necessity of performing a consistent comparative study, TPS data were compared against the corresponding MC simulation (dose to water for all simple algorithms and for AAA-ECL and MGS-XiO and dose to tissue for the two CC) and all results presented in the following will implicitly assume this condition.

For reasons of space, in this paper only a subset of the analysed data is shown in the figures and in the tables. More figures and tables are included in the complementary material associated with this paper and available in electronic format on the journal's web site (in the following, tables and figures from this material will be referenced with a subscript 'cmp').

3. Results and discussions

3.1. Validation of the beam's characteristics in water

The beam's characteristics (as reproduced by the different calculation algorithms) used for all dose calculations were considered as sufficiently homogeneous for the purposes of the study. The observed spread in beam quality of $TPR_{20/10}$ was less than 1% at average (at one standard deviation) as reported in table 1. Also the validation performed on the conventional fields in water proved adequate matching among all beams. In average, differences in depth dose were smaller than 1% (or 1 mm) and 2% for profiles with the exceptions of CC-TMS at 15 MV in the build-up region and for the MC simulations at 15 MV (not fully reproducing the infield shoulders), in both cases agreement was within 3 mm or 3% (better for 6 MV than for 15 MV).

In figure 1_{cmp}, as an example, for the reference field 10×10 cm^2, the depth dose curves are reported for all type-b algorithms. Regarding the profiles, the same field at 10 cm depth is represented as difference between the TPS calculated profile (or ion chamber measurement) and the Monte Carlo simulation. As can be seen, within the clinical field size no significant difference was present. Some differences were observed in the tails where the different head scatter models become more important (e.g. the MC simplified simulation does not incorporate full modelling of head scatter). These differences were, however, not relevant for the present investigations. Concerning the profile penumbra (defined as distance between the 20% and the 80% relative dose), the MC simulation presented smaller values with respect to the TPS calculated ones of about 3 mm for the 6 MV, and 2 mm for the 15 MV quality.

A γ index evaluation on same field sizes, energies and profiles was conducted also in a completely homogeneous (water) phantom for two type-a (PBC-ECL and PB-TMS) and for two type-b algorithms (AAA-ECL and CC-TMS). The fraction of point with $\gamma < 1$ was about 0.9 with $\Delta D = 3\%$

3.2. Depth doses and profiles

In figures 2 and 3 depth dose curves are presented for the two beam qualities and for the two field sizes, at 4 cm off-axis on each side of the heterogeneous insert, i.e. the light lung, normal lung and bone. The latter was divided into $bone_w$ and $bone_t$ according to the MC simulation used for comparison. Vertical lines on the graphs correspond to the interfaces between different densities.

Figure 4 reports, similarly to the previous ones but for the 13×13 cm^2 field only, the depth doses at 0.8 cm off-axis on the homogeneous side of the phantom, while figure 5 presents the symmetric condition on the heterogeneity side (splitting the bone case as described above).

Figures 6 and 7 present transverse profiles at the mid-depth of the heterogeneous insert ($d =$ 13 cm for light and normal lung, and $d = 7$ cm for the bone case) for the different densities, energies and field sizes.

In the complementary material, figures 2_{cmp} and 3_{cmp} show depth dose curves for the 2.8×13 cm^2 field at 0.8 cm off-axis in water and in the heterogeneous insert respectively. Figures 4_{cmp}, 5_{cmp} and 6_{cmp} show transverse profiles at different depths: 1 cm inside the proximal edge of the insert, 2 cm before the end of the insert, and 1 (2) cm after the distal edge of the insert for lung (bone), in water. Only the 13×13 cm^2 case is given, results for the 2.8×13 cm^2 are similar.

There was a systematic difference in behaviour, well visible in the depth dose curves for low density media, between type-a (PBC-ECL, PB-TMS and FFTC-XiO) and type-b (CC-TMS, CC-PIN, MGS-XiO and AAA-ECL) algorithms. In the bone case, differences among all algorithms seem to be quantitatively small while there was a clear qualitative separation

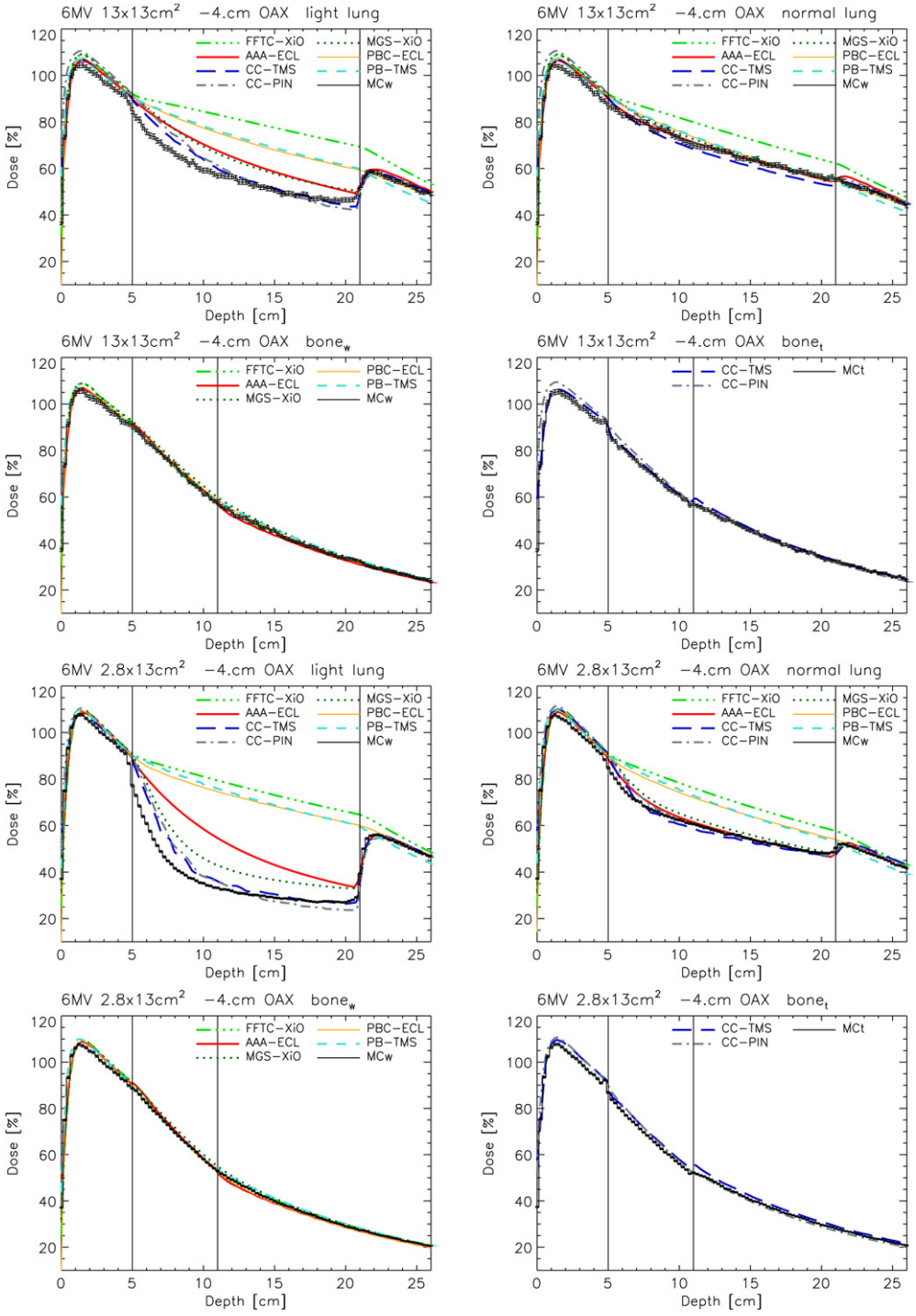

Figure 2. Depth dose curves for the 6 MV calculations, at 4 cm off-axis on the heterogeneity side. Graphs are subdivided according to density (light and normal lung, bone as water and tissue) and field size (13 × 13 cm^2 and 2.8 × 13 cm^2). All algorithms and MC simulations are shown.

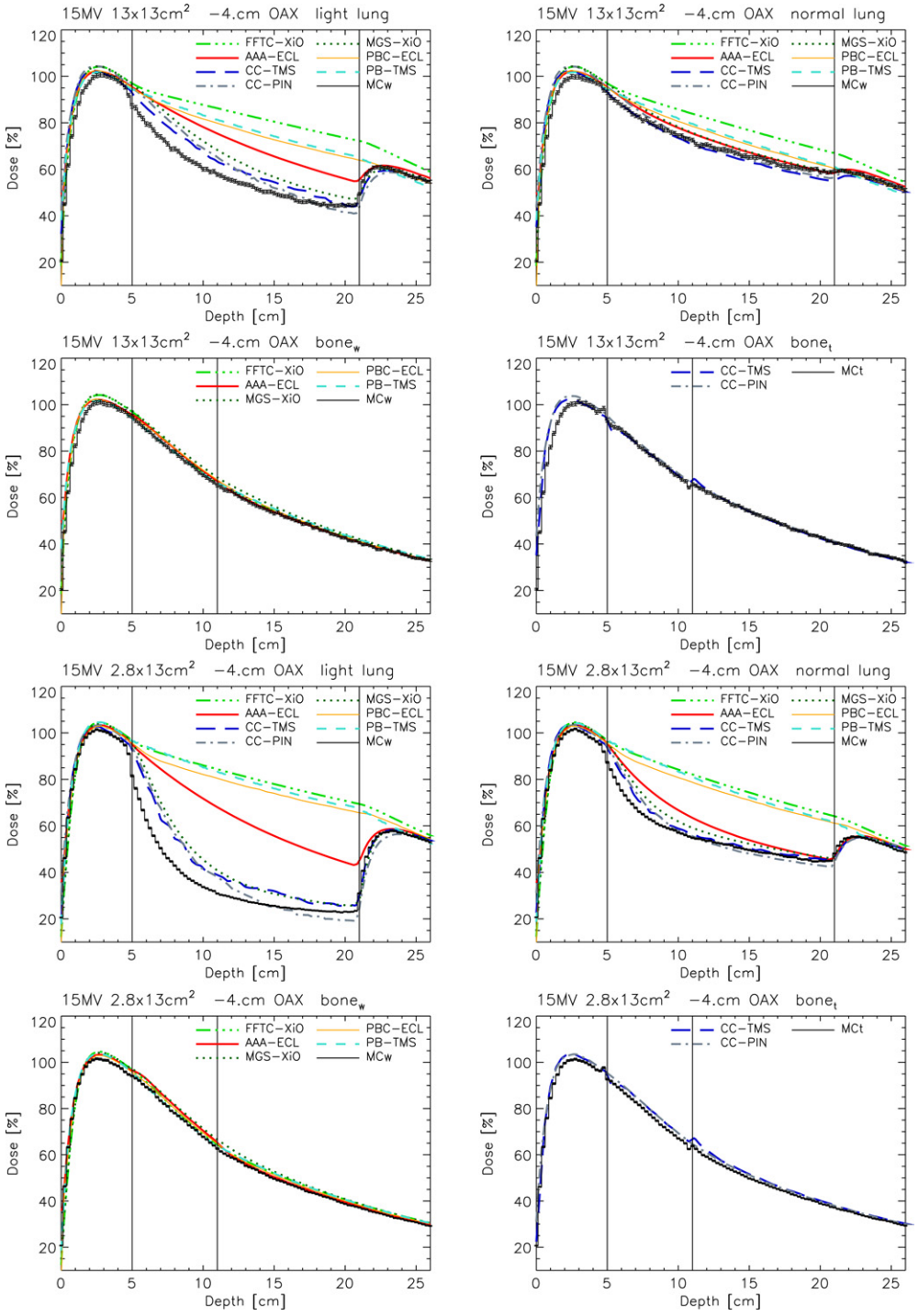

Figure 3. Depth dose curves for the 15 MV calculations, at 4 cm off-axis on the heterogeneity side. Graphs are subdivided according to density (light and normal lung, bone as water and tissue) and field size (13 × 13 cm^2 and 2.8 × 13 cm^2). All algorithms and MC simulations are shown.

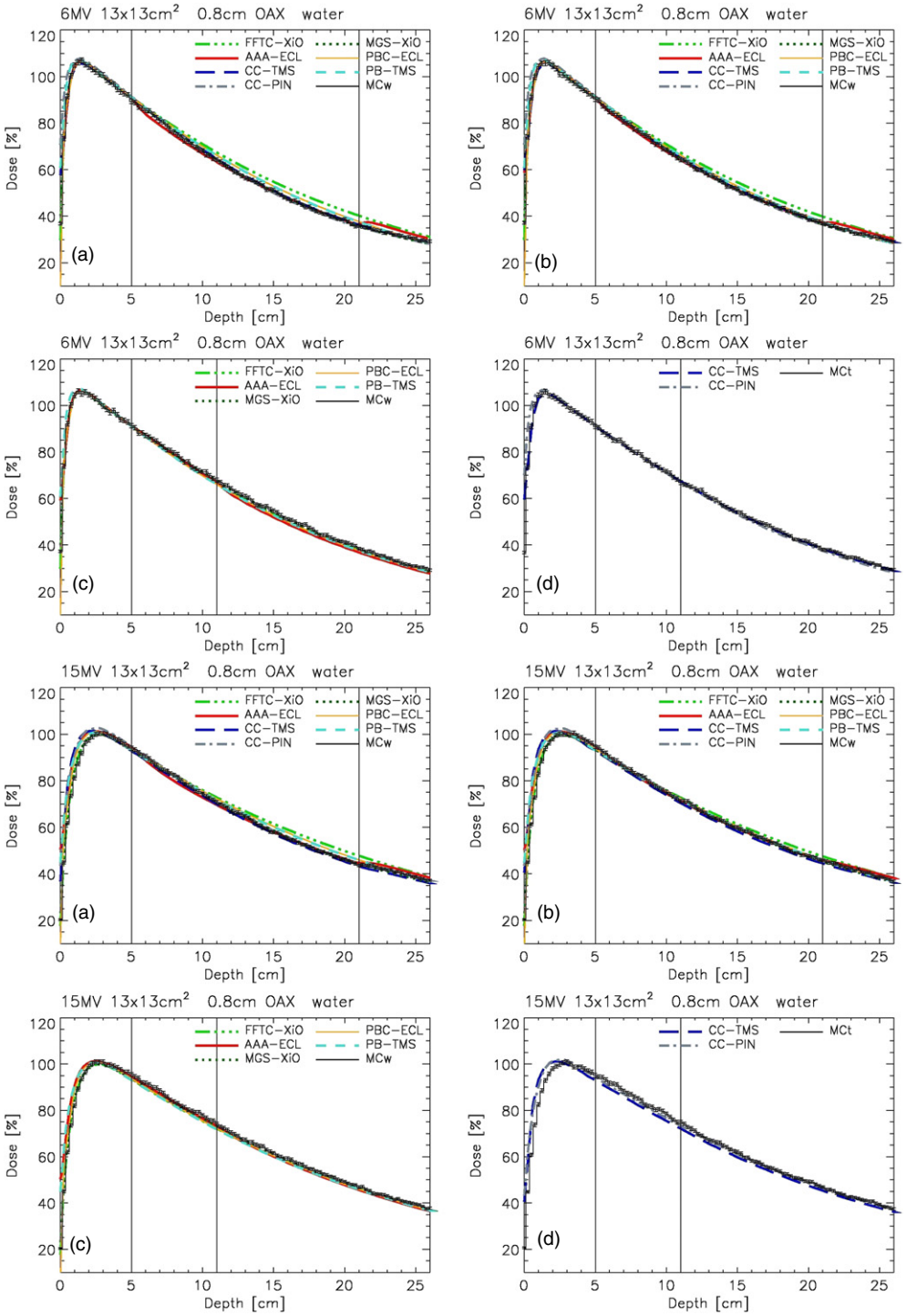

Figure 4. Depth dose curves for the field 13 × 13 cm^2 at 0.8 cm off-axis on the water side. Graphs are subdivided according to density ((a) light lung, (b) normal lung, (c) bone as water and (d) bone as tissue) and energy. All algorithms and MC simulations are shown.

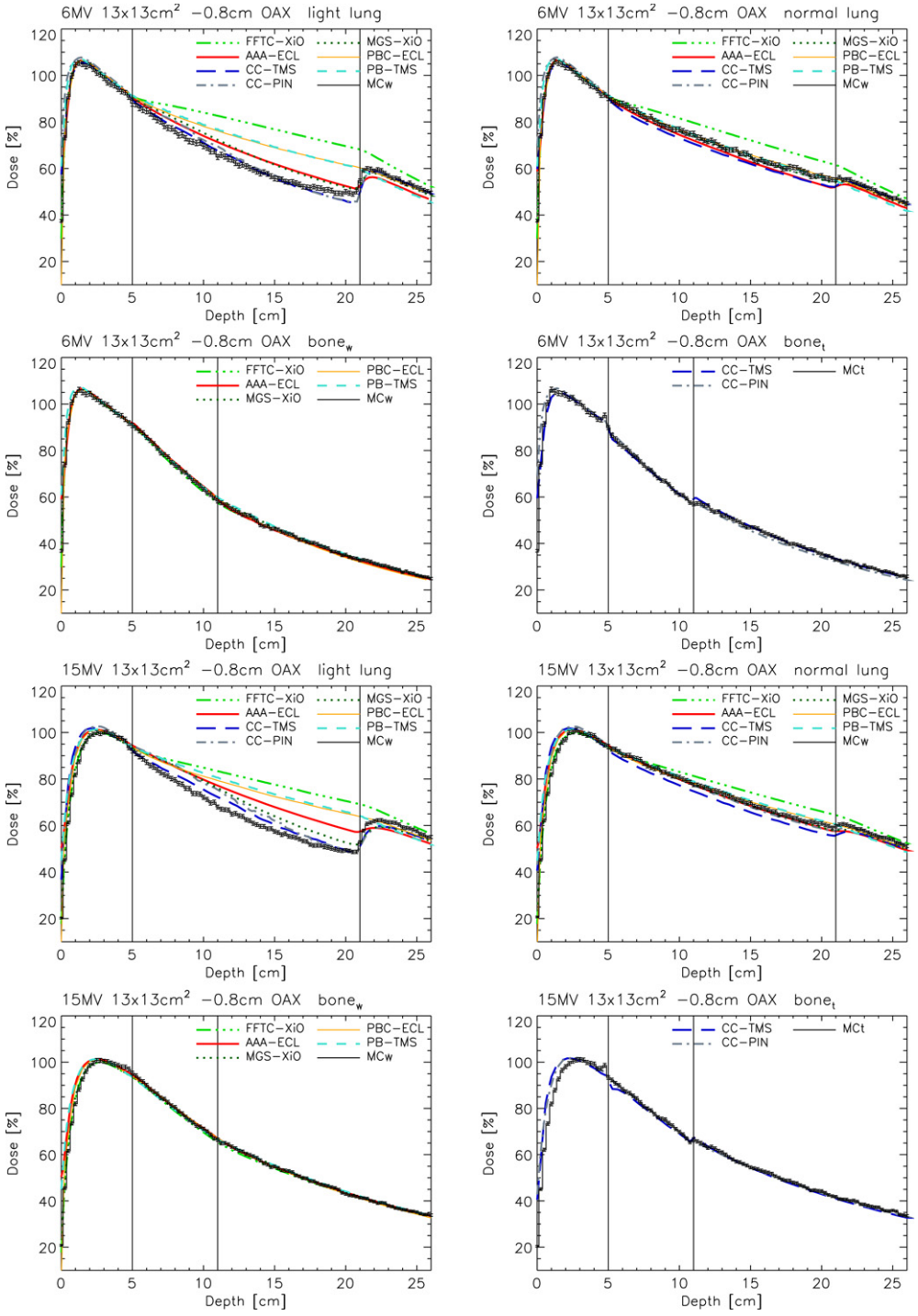

Figure 5. Depth dose curves for the field 13 × 13 cm^2 at 0.8 cm off-axis on the heterogeneity side. Graphs are subdivided according to density (light and normal lung, bone as water and tissue) and energy (6 and 15 MV). All algorithms and MC simulations are shown.

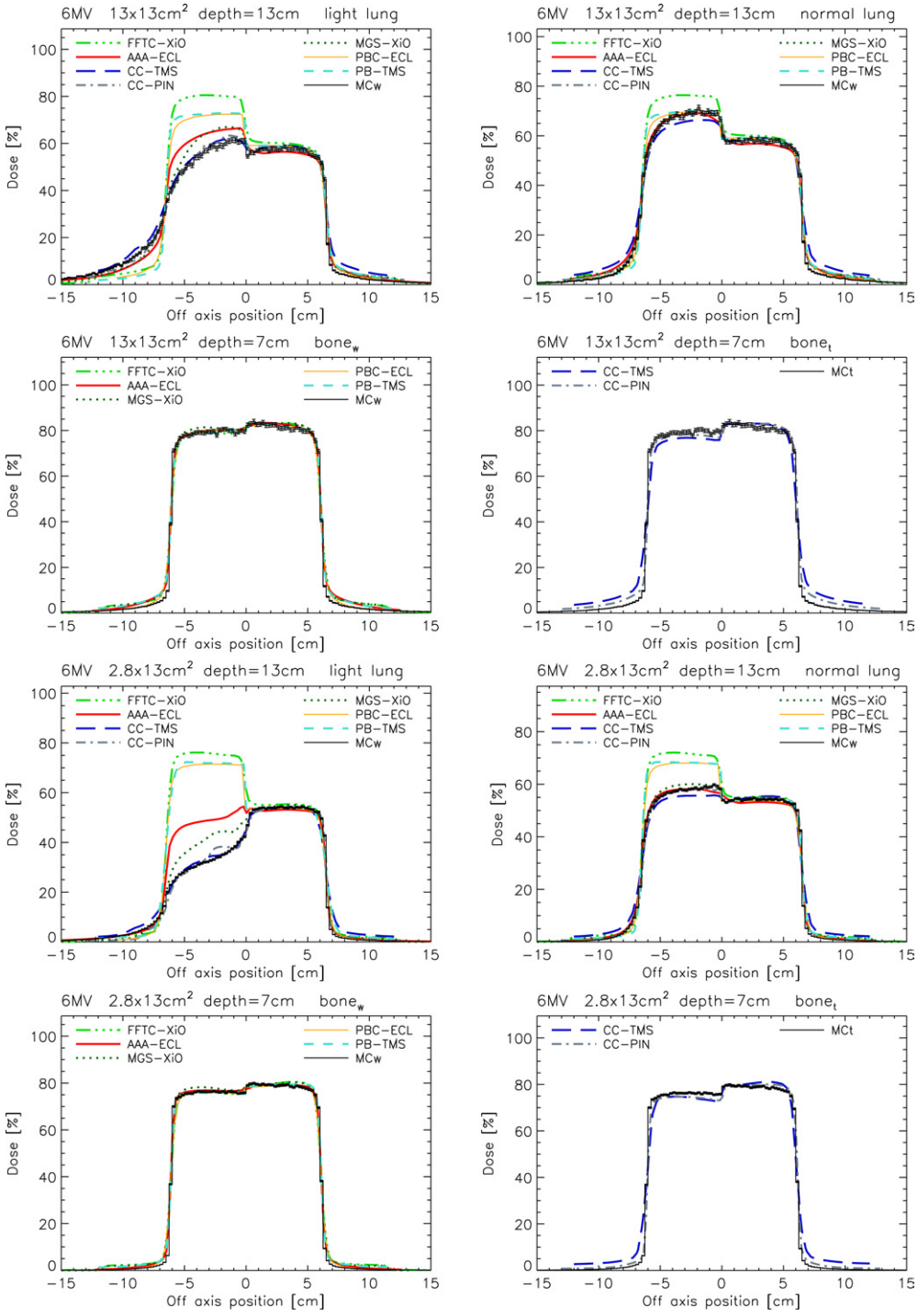

Figure 6. Profile curves for the 6 MV calculations, at the central depth of the insert. Graphs are subdivided according to density (light and normal lung, bone as water and tissue) and field size (13×13 cm^2 and 2.8×13 cm^2). All algorithms and MC simulations are shown.

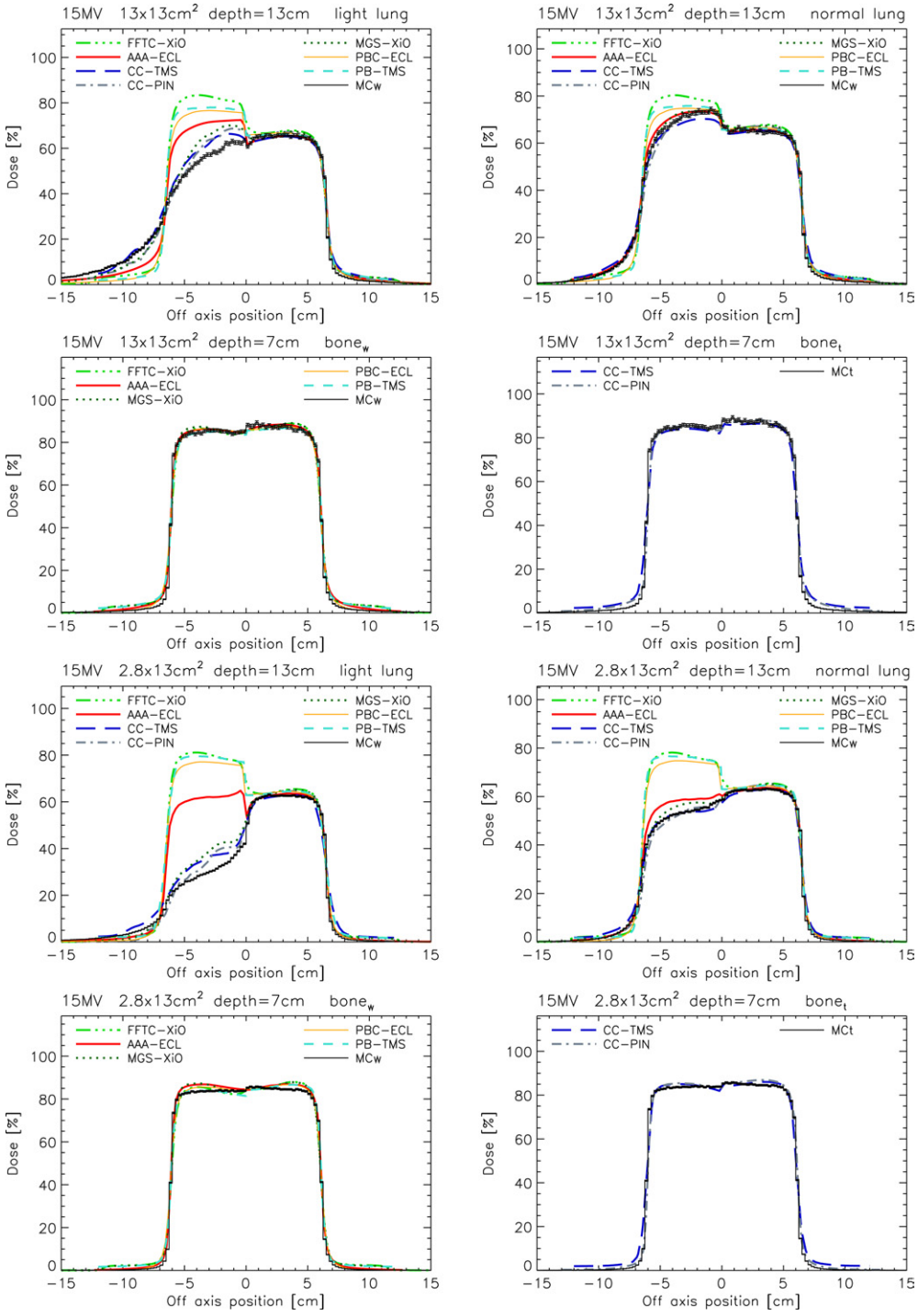

Figure 7. Profile curves for the 15 MV calculations, at the central depth of the insert. Graphs are subdivided according to density (light and normal lung, bone as water and tissue) and field size (13×13 cm^2 and 2.8×13 cm^2). All algorithms and MC simulations are shown.

between the models computing dose to water or dose to tissue. Some of type-a algorithms completely fail to account for the presence of non-water material out of the ray-path, leading to a poor estimation of the dose inside a medium with density lower than water. For all algorithms, narrow rectangular fields (like the 2.8 × 13 cm^2) were similarly managed as the larger square fields (as the 13 × 13 cm^2).

3.3. Considering the light lung experiment

(i) Type-a algorithms presented, as expected, an important overestimation of the calculated dose inside the heterogeneity, much more pronounced for the small fields. Another point to consider is the absence of the re-buildup after the heterogeneity (clearly more important at higher energies).

(ii) Amongst type-b algorithms, the two collapsed cone implementations (CC-TMS and CC-PIN) and the MGS-XiO (that is substantially a collapsed cone algorithm implementing a speed utility where the convolution is performed on a coarse grid when no gradients in density of fluence are present) present mainly a consistent behaviour, confirming the belonging in principle to the same algorithm. All three CC doses were higher than the MC simulated dose in most of the curves. A difference was found for some cases for depths larger than 5–7 cm in the heterogeneity, where the CC-TMS/PIN curves start to mutually diverge, with the CC-PIN calculating a slightly smaller dose. The MGS-XiO algorithm at 15 MV behaves very similarly to the other CC, while at 6 MV it calculates a significantly higher dose.

(iii) The result for the AAA algorithm was in most cases at an intermediate position between MC (and CC) and the pencil-beam calculations with a slightly smaller discrepancy for the lower energy.

(iv) All the algorithms showed for this extremely low density, a radial dependence: DD computed at 4 cm off-axis (figures 2 and 3) were in general worse than DD computed at 0.8 cm off-axis (figure 5) independently from the energy and, less evident, from field size (figures 2, 3 and 3_{cmp})

Nevertheless, the light lung experiment was a sort of extreme case, of very limited clinical relevance for large thickness; however, since a density of 0.035 g cm^{-3} is found only in small cavities as possibly paranasal sinuses. The relevance of the experiment was to study the algorithms where the heterogeneity modelling was pushed into such extreme conditions where it may fail.

Considering the intermediate experiment, *the normal lung* case, the following considerations apply.

(i) As for the light lung case, FFTC-XiO, PB-TMS and PBC-ECL failed to consider densities different from unity out of the ray path, more evidently for narrow than for large beams, and more pronounced at the higher photon energy.

(ii) All type-b algorithms presented a better agreement to MC for both energies in the case of the 13 × 13 cm^2 field, and for the small field in the low energy case. For the 2.8 × 13 cm^2 field and 15 MV the algorithms based on the collapsed cone were more consistent with MC than the AAA model.

(iii) The dependence on off-axis distance was present but almost negligible if compared to the previous experiment and no major differences were seen for DD computed at 4 cm or 0.8 cm. In fact, all type-b and most type-a algorithms, work acceptably for large beams as long as lateral charged particle equilibrium is established. Increasing energy or narrowing the beam stress the models and the simpler ones failed to reproduce MC simulations since

no electron modelling was considered. The methods used by the CC algorithms were more robust.

In the case of *bone* the following considerations apply.

(i) A fairly good agreement was observed for all algorithms, also for type-a algorithms.
(ii) Both the CC algorithms, but more evident for the CC-TMS, two 'discontinuities' were present at the insert interfaces. At the proximal edge the CC curve showed a 'fall' after a small peak just before the heterogeneity while at the distal edge, a sort of 'build-down' was visible in the last layers of bone followed by a 'build-up' inside water (well visible in figure 3 but present in all other cases). This feature was qualitatively and quantitatively consistent with the MC simulation performed in tissue and it is consistent with what has been reported in the literature (e.g. Nisbet *et al* (2004), Bedford *et al* (2003)). It essentially originates by the discontinuous changes in radiation transport (e.g. changes in stopping-power ratios and in energy transfer coefficients) between water and other tissues (in this case bone) at the interfaces. A similar behaviour was absent when dose-to-water calculations were performed as in the case of AAA-ECL or MGS-XiO. It should be extremely important to define a general consensus among TPS developers and scientific bodies to converge to a unique method of dose computation, consistent with definitions, in order to minimize or avoid biases, interpretation and compatibility problems when analysing data from different systems. As this is not the case we can only recommend that both possibilities should be available when appropriate.

Concerning DD computed in the homogeneous water part of the phantom, there was a general satisfactory agreement between all algorithms and MC, at least within the intrinsic limits of similar experiments. To mention, in the case of AAA, after the distal edge of the insert, the presence of a re-buildup was visible also on the water side (e.g. figures 4 and 2_{cmp} for the light lung and, slightly, for the normal lung cases). This feature points to a possibly excessive weight of points contributing to the superposition situated at relatively large radial distances from the calculation point in addition to the fact that, changes in photon scatter on the heterogeneity side may influence the water side.

Concerning lateral profiles shown in figures 6, 7, 4_{cmp}, 5_{cmp} and 6_{cmp}, it is important to note the shallower tail of AAA in the transition from lighter to more dense materials as discussed above and possibly due to an overestimation of distant contributions to the superposition phase. In all cases, the discrepancies, present outside the nominal field edges and more pronounced in the lighter densities, shall not be considered since they are not pertinent to the purposes of the study, and are mostly due to different modelling of head scattering in the different algorithms and MC simulation, and not truly linked to the heterogeneity management mechanisms. In any case, those regions were not considered in the calculation of the γ index.

3.4. The γ index analysis

Using the MC simulation as a reference and stratifying the investigation for the field areas inside or outside of the heterogeneity, it was possible to compute the γ index for 425 points in water and for 156 points for each non-unity density group (65 for the bone case) varying the threshold in dose (ΔD). Figures 7_{cmp} (a) and (b) show, as an example, the histograms of the γ index distribution evaluated for the normal lung case with DTA = 3 mm and $\Delta D = 3\%$ for the field 13×13 cm^2 and for both photon beam qualities. The parameter 'γ agreement index', γAI, has been defined as the histogram area corresponding to $\gamma < 1$ which was the fraction of points considered acceptable in the γ evaluation. This parameter represents the ability of a specific algorithm in specific conditions to reproduce MC simulations.

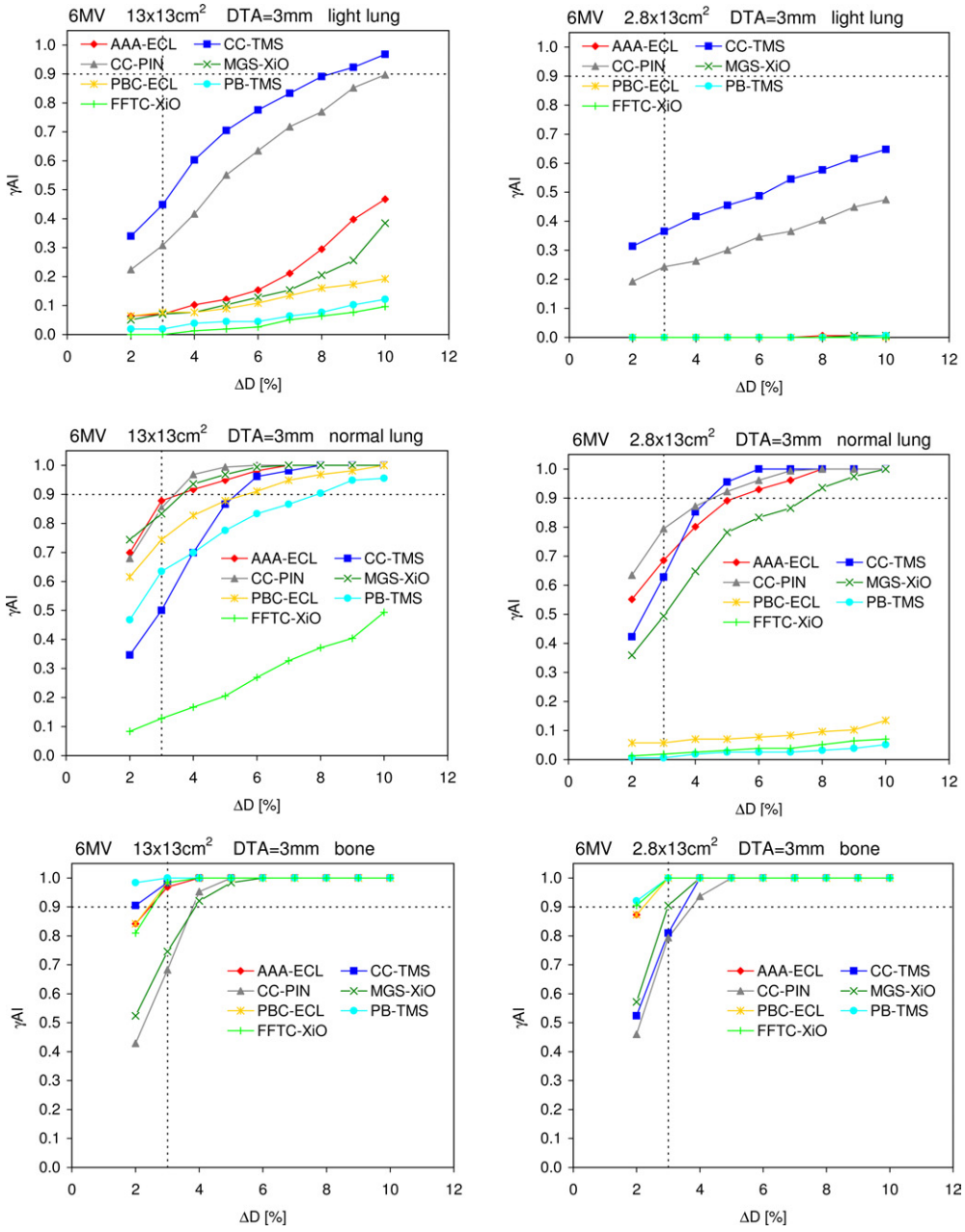

Figure 8. Summary of the γ index analysis (with fixed DTA = 3 mm) for the calculation points falling inside the inserts different from water. For each graph it is shown in ordinate the fraction of points resulting with $\gamma < 1$ (γAI) and in abscissa ΔD. Data are shown for 6 MV.

In figures 8 and 9 the final results for the γ index analysis are presented. For each algorithm, density, energy and field size, the variation of γAI is shown as a function of ΔD. Results are shown only for the point falling within the heterogeneous inserts. In the figures, the dashed lines correspond to two interesting conditions: the vertical line is for the gamma

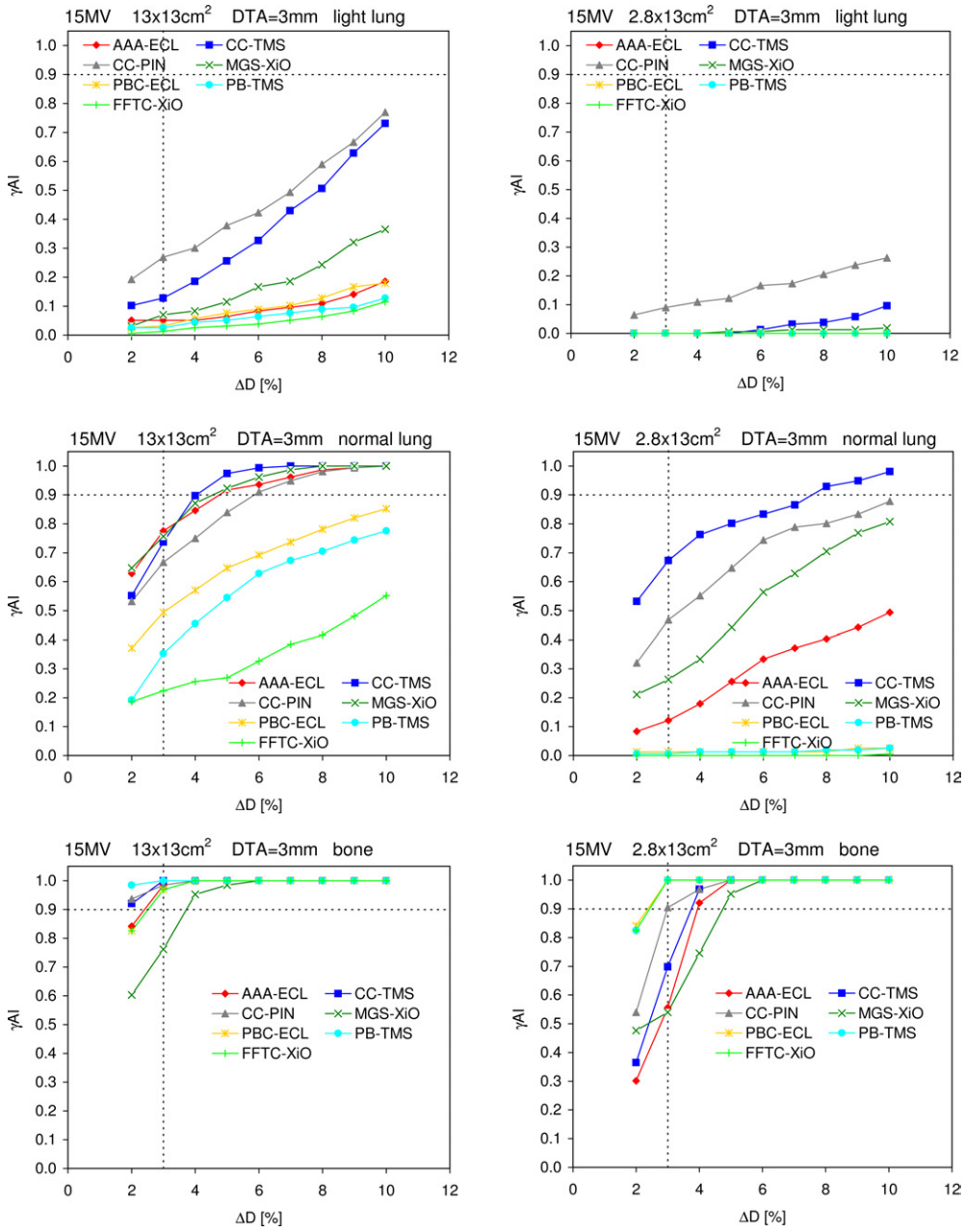

Figure 9. Summary of the γ index analysis (with fixed DTA = 3 mm) for the calculation points falling inside the inserts different from water. For each graph it is shown in ordinate the fraction of points resulting with $\gamma < 1$ (γAI) and in abscissa ΔD. Data are shown for 15 MV.

analysis with DTA = 3 mm and $\Delta D = 3\%$, a commonly accepted set of thresholds, indicating the relative performances of algorithms in conditions comparable with other publications. The horizontal lines correspond instead to an ideal agreement index of 0.90, i.e. the case where for 90% of the analysed points the MC simulation and TPS calculation would show $\gamma < 1$.

Table 2. Index of agreement γAI (fraction of points with $\gamma \leqslant 1$) for DTA = 3 mm and $\Delta D = 3\%$.

		Light lung case				Normal lung case				Bone case			
Energy		Light lung		Water		Normal Lung		Water		Bone[c]		Water	
Field size	Algorithm	γAI	γAI[a]	γAI	γAI[b]	γAI	γAI[a]	γAI	γAI[b]	γAI	γAI[a]	γAI	γAI[b]
6 MV	AAA-ECL	0.07	0.14	0.75	0.80	0.88	1.00	0.77	0.56	0.97	0.90	0.65	0.44
13 × 13 cm^2	CC-TMS	0.45	0.24	0.74	0.94	0.50	1.00	0.78	0.96	0.98	1.00	0.92	0.87
	CC-PIN	0.31	0.14	0.78	0.86	0.85	0.86	0.79	0.86	0.68	0.48	0.66	0.98
	MGS-XiO	0.07	0.14	0.78	0.94	0.83	0.57	0.80	0.94	0.75	0.71	0.91	0.91
	PBC-ECL	0.08	0.14	0.84	0.90	0.74	0.67	0.87	0.88	0.98	1.00	0.84	0.91
	PB-TMS	0.02	0.05	0.71	0.62	0.63	0.67	0.76	0.58	1.00	1.00	0.82	0.82
	FFTC-XiO	0.00	0.00	0.34	0.16	0.13	0.38	0.42	0.22	0.98	1.00	0.89	0.91
6 MV	AAA-ECL	0.00	0.00	0.80	0.56	0.69	0.29	0.83	0.60	1.00	1.00	0.65	0.58
2.8 × 13 cm^2	CC-TMS	0.37	0.00	0.88	0.98	0.63	0.52	0.62	0.68	0.81	0.76	0.87	0.87
	CC-PIN	0.24	0.00	0.87	0.66	0.79	0.24	0.89	0.94	0.79	0.57	0.66	0.91
	MGS-XiO	0.00	0.00	0.89	0.70	0.49	0.05	0.93	0.90	0.90	0.95	0.95	0.82
	PBC-ECL	0.00	0.00	0.89	0.80	0.06	0.00	0.90	0.88	1.00	1.00	0.61	0.73
	PB-TMS	0.00	0.00	0.68	0.40	0.01	0.00	0.80	0.70	1.00	1.00	0.85	0.84
	FFTC-XiO	0.00	0.00	0.67	0.42	0.02	0.00	0.74	0.50	1.00	1.00	0.95	1.00
15 MV	AAA-ECL	0.05	0.10	0.75	0.88	0.78	0.62	0.77	0.90	0.98	1.00	0.84	0.96
13 × 13 cm^2	CC-TMS	0.13	0.19	0.74	0.82	0.74	0.95	0.78	0.92	1.00	1.00	0.82	1.00
	CC-PIN	0.27	0.14	0.69	0.48	0.67	1.00	0.79	0.82	0.98	1.00	0.86	0.98
	MGS-XiO	0.07	0.10	0.63	0.60	0.76	0.62	0.71	0.82	0.76	0.81	0.75	0.73
	PBC-ECL	0.03	0.14	0.75	0.80	0.49	0.67	0.82	0.96	0.97	1.00	0.85	1.00
	PB-TMS	0.03	0.10	0.73	0.76	0.35	0.62	0.76	0.88	1.00	1.00	0.79	0.80
	FFTC-XiO	0.01	0.10	0.38	0.16	0.22	0.52	0.48	0.32	0.97	0.90	0.82	0.93
15 MV	AAA-ECL	0.00	0.00	0.79	0.62	0.12	0.00	0.84	0.86	0.56	1.00	0.90	0.98
2.8 × 13 cm^2	CC-TMS	0.00	0.00	0.78	0.94	0.67	0.10	0.83	0.84	0.70	0.90	0.76	0.78
	CC-PIN	0.09	0.00	0.52	0.30	0.47	0.00	0.61	0.50	0.90	0.90	0.90	0.96
	MGS-XiO	0.00	0.00	0.60	0.48	0.26	0.00	0.64	0.60	0.54	0.90	0.58	0.47
	PBC-ECL	0.00	0.00	0.73	0.38	0.01	0.00	0.82	0.46	1.00	1.00	0.96	0.98
	PB-TMS	0.00	0.00	0.86	0.50	0.01	0.00	0.77	0.54	1.00	0.95	0.73	0.69
	FFTC-XiO	0.00	0.00	0.38	0.06	0.00	0.00	0.44	0.22	1.00	0.95	0.58	0.64

[a] Fraction of points with $\gamma \leqslant 1$ at a depth of 1 cm after the beginning of the heterogeneous insert ($d = 6$ cm).
[b] Fraction of points with $\gamma \leqslant 1$ at a depth of 1 cm after the end of the heterogeneous insert ($d = 22$ cm for light lung and normal lung, $d = 13$ cm for the bone case).
[c] For the bone case, AAA-ELC, MGS-XiO, PBC-ECL, PB-TMS and FFTC-XiO were compared against the simulation performed in water with scaled density ($bone_w$) while for CC-TMS and CC-PIN the comparison was compared against the corresponding simulation in tissue ($bone_t$).

In this case it is possible to identify the threshold in ΔD necessary to reach (if possible) this global objective.

In table 2, the γAI values are reported for the case DTA = 3 mm and $\Delta D = 3\%$. In that table all photon energies, field sizes and algorithms are presented for all three densities. For each case, two γAI values are reported for the analysis inside the heterogeneity: the first takes into account all the points in the field inside the insert, while the second one reports the result of the profiles located at 1 cm depth in the insert itself ($d = 6$ cm). In the same way, two γAI values are reported for the points in water (for all density experiments): one considering all the points located in the water part of the phantom, and the other one reporting the result of the profiles located at 1 cm depth after the heterogeneity insert. In this way, it is possible to

evaluate if there is a major difference, for a specific case and algorithm, in the first centimetre of different density that could be in principle clinically interesting.

The γ analysis, summarized in figures 8 and 9, allows some general conclusions.

(i) The light lung ($\rho = 0.035$ g cm^{-3}) is extremely difficult to manage for all algorithms. Only the CC algorithms had a potential of modelling the dose in this extreme case (TMS better than Pinnacle for 6 MV) reaching values of γAI larger than 0.5 in most of the cases. For ΔD greater than 8–9%, γAI reached the ideal threshold of 0.90 in the large field cases at low energy. For small fields, and particularly for 15 MV, γAI values were extremely low and clearly not satisfactory for any of the studied algorithms.

(ii) The condition of normal lung ($\rho = 0.20$ g cm^{-3}) presented more complicated patterns and data were significantly spread. For small fields at low energy there was a clear separation between type-a and -b algorithms: the advanced reach γAI $= 0.90$ at $\Delta D \sim 4\%$ (CC-TMS and CC-PIN), $\Delta D \sim 5\%$ (AAA-ECL) and $\Delta D \sim 7.5\%$ (MGS-XiO). At high energy, the separation among type-a and -b algorithms was still present but there was also a significant spread among type-b. CC-TMS was the only algorithm capable of reaching γAI $= 0.90$ with $\Delta D \sim 7.5\%$. The worst result among type-b algorithms was given by AAA-ECL, not reaching γAI $= 0.90$ even for $\Delta D = 10\%$.

For large fields, the separation between type-a and -b algorithms was still significant at 15 MV where PB-ECL, PB-TMS and FFTC-XiO never reached γAI $= 0.90$ with ΔD up to 10% while type-b algorithms reached this threshold for ΔD between 4% (CC-TMS) and 6% (CC-PIN). The data for the 6 MV case were similar with type-b algorithms reaching γAI $= 0.90$ for ΔD between 3% and 4% (with the exception of CC-TMS at $\sim$5.5%).

As a global summary, it is relevant to note that there is no algorithm capable of performing adequately under all conditions, still suggesting a relatively weak reliability of all algorithms in the most important case for clinical applications, especially for high energies.

(iii) The last case with a heterogeneity simulating cortical bone ($\rho = 1.80$ g cm^{-3}) presented generally good results for all algorithms and a clear tendency to reach γAI > 0.90 for ΔD thresholds in the range of 2–4%. As for the other experiments, the small fields were revealed to be more critical, particularly at 15 MV for ΔD values lower than 5%.

As a final summary, based on DTA $= 3$ mm and $\Delta D = 3\%$, considering the four type-b algorithms, the agreement indices computed averaging results for energies and field sizes for the most clinically interesting case of the normal lung were as follows: CC-PIN (0.70 ± 0.17), CC-TMS (0.63 ± 0.10), AAA-ECL (0.62 ± 0.34) and MGS-XiO (0.59 ± 0.26). Averaging the results also over all the densities the global means of the agreement index for type-b systems were CC-PIN (0.59 ± 0.30), CC-TMS (0.58 ± 0.31), AAA-ECL (0.51 ± 0.43) and MGS-XiO (0.45 ± 0.35). It is important to note that most of the differences between algorithms were not statistically significant due to the partial overlap of uncertainties and therefore cannot be used to draw absolute conclusions but could be helpful to identify areas of weakness or strength to be further investigated according to individual clinical needs or interests.

Looking at data relative to type-a algorithms, the average agreement indices from all experiments were: PBC-ECL (0.45 ± 0.46), PB-TMS (0.42 ± 0.47) and FFTC-XiO (0.36 ± 0.47). Limiting the average to the normal lung case only, the values were PBC-ECL (0.33 ± 0.35), PB-TMS (0.25 ± 0.30) and FFTC-XiO (0.09 ± 0.10). Restricting the evaluation to the small fields, all the three type-a algorithms presented γAI less than 0.05.

For points falling inside the uniform water medium a rather good agreement was observed between all algorithms and MC. For the $\Delta D = 3\%$ threshold the agreement indices averaged

over all configurations ranged from 0.59 ± 0.22 (FFTC-XiO) to 0.82 ± 0.09 (PBC-ECL), without identified trends or patterns.

As a final remark it is important to mention that calculation speed was not possible to evaluate in a consistent way in the present study since the TPS analysed were used in a variety of computer environments hardly comparable in absolute terms, especially because of their intrinsic different hardware. Nevertheless it is interesting to report a qualitative summary based on relative indications, which can be done for those systems including both a type-a and a type-b algorithm. For these systems computation times were investigated for fixed clinical conditions (calculation grid, field size, CT sampling). These calculation times were nevertheless still depending upon more parameters specific to the systems, and therefore should be extrapolated with care. For the small field condition used in the present study, the time ratio between type-a and -b algorithms ranged from a factor lower than 2 for Eclipse (AAA versus pencil beam) to a factor 10–15 for TMS (CC versus pencil beam) and XiO (MGS versus FFTC). Preliminary information, derived mainly from the manufacturer's private communication, suggest that forthcoming releases of these 'slower' algorithms could reduce the ratio to a factor ∼4 or better. Pinnacle was not tested in this sense since in its clinical release only a type-b algorithm is accessible for testing. For clinical applications, however, the speed of calculation is a relevant and sometimes limiting factor for some algorithms and should be considered with care by manufacturers as a key factor for the global success of any algorithm.

4. Conclusion

A comparative study was performed to investigate performances of several dose calculation algorithms for photon beams applied to simple phantoms simulating non-homogeneous media. Two groups of algorithms were identified: the 'simpler' (type-a), where electron transport is not modelled, and 'more advanced' (type-b), where, in an approximate way, electron transport is taken into account.

Results confirmed the inadequacy of the algorithms belonging to the first category to manage dose calculation inside heterogeneous media, especially for small fields in low density media. For the second group results were more contradictory and depend upon beam energy, field size and density investigated. From the most clinically relevant case (the normal lung) it shall be concluded that

(i) type-b algorithms have been found to be preferable to simple models and therefore should always be used in clinical practice;
(ii) pressure should still be put on industry to complete the evolution of dose calculation algorithms and solve residual problems;
(iii) calculation speed and other issues related to routine practice should be included in a multi-factorial evaluation if strategic decisions shall be taken in any institute.

Acknowledgments

The Lund University Hospital research funds and the Oncosuisse (grant OCS 01821-02-2006) are greatly acknowledged for their financial support together with all colleagues at the participating departments.

Appendix

The PB-TMS is a pencil-beam convolution/superposition model based on energy fluence. It convolves a 2D fluence matrix with pre-calculated pencil beams. Head scatter is treated

separately. Inhomogeneities are handled by an EPL correction for the primary dose contribution and by a one-dimensional convolution with an exponential for scattered radiation (Ahnesjö and Trepp 1991, Ahnesjö *et al* 1992). The pencil beam is parametrized at every 0.25 cm along the direction of propagation.

The PBC-ECL from Varian Eclipse is similarly based on the convolution/superposition principle. The pencil beam is parametrized at five depths and accordingly the convolution with the incoming fluence is performed only at these depths while interpolation occurs in-between. The pencil beams are extracted from measurements. Details are given in Storchi and Woudstra (1996) and Storchi *et al* (1999). In this study, heterogeneity management was performed according to the modified Batho (Webb and Fox 1980) method. This method only considers density variation along the fan line, i.e. it is an EPL-based method and does not account for changes in lateral electron transport.

The FFTC-XiO from CMS is a point kernel which is convolved with the TERMA distribution. The convolution is performed in the frequency domain by means of fast Fourier transform thus no correction for density is performed. The TERMA calculation, however, considers density variations during the ray tracing. The system also includes a head scatter model (Miften *et al* 2000).

The CC-TMS from Helax-TMS is a collapsed cone convolution algorithm. The TERMA (total energy released per unit mass) is computed in all points considering the ray trace through the irradiated volume, and it is transported away along about 100 directions. The TERMA (separated in primary and scattered, Ahnesjö *et al* (2005)) is deposited according to the elemental composition of each voxel (Ahnesjö 1989). Dose kernels computed in CC-TMS are produced by the EGS4 Monte Carlo code (Mackie *et al* 1988).

The CC-PIN implemented in Pinnacle is also a collapsed cone convolution algorithm developed by the Madison group in parallel with the Ahnesjö group. This implementation is very similar to the HELAX CC except it does not separate the TERMA into primary and scatter. It is well described by Papanikolaou *et al* (1993) and McNutt *et al* (1996).

The AAA-ECL implemented in the Eclipse system is based on a pencil-beam convolution/superposition technique. The pencil beam is derived from Monte Carlo calculations and adjusted to fit measurements. In this case, the longitudinal distribution of the pencils are scaled with the radiological depth (EPL). The lateral extensions of the pencil beams are scaled with the density relative to water in directions normal to the pencil beam by applying six independent (anisotropic) exponential absorption functions. In this way the changes in lateral transport of energy are modelled when the density varies in the irradiated object (Ulmer and Harder 1995, 1996, 2005). Scaling with depth is further modelled by two additional exponential functions along the z direction.

The MGS-XiO implemented in XiO from CMS has been described by Miften *et al* (2000, 2001) and includes a head scatter model. The algorithm uses a point kernel representing the dose transport which is convolved with the ray-traced TERMA distribution. The dose kernel comes from the same data set as CC-TMS and CC-PIN. During integration, the kernel is modified according to density. The main difference from the other CMS algorithm is that this model uses a variant kernel instead of the invariant point kernel used in the FFT convolution. The term multigrid comes from the use of a varying resolution of the calculation grid depending on potential dose gradients i.e. at high density gradients and at beam edges.

References

AAPM Report 85 2004 Tissue inhomogeneity corrections for MV photon beams *Report of Task Group No. 85 of the Radiation Therapy Committee of the American Association of Physicists in Medicine (AAPM)* (Madison, WI: Medical Physics Publishing)

Ahnesjö A 1989 Collapsed cone convolution of radiant energy for photon dose calculation in heterogeneous media *Med. Phys.* **16** 577–92

Ahnesjö A, Saxner M and Trepp A 1992 A pencil-beam model for photon dose calculation *Med. Phys.* **19** 263–73

Ahnesjö A and Trepp A 1991 Acquisition of the effective lateral energy fluence distribution for photon beam dose calculations by convolution models *Phys. Med. Biol.* **36** 973–85

Ahnesjö A, Weber L, Murman A, Saxner M, Thorslund I and Traneus E 2005 Beam modeling and verification of a photon beam multisource model *Med. Phys.* **32** 1722–37

Aspradakis M M, Morrison R H, Richmond N D and Steele A 2003 Experimental verification of convolution/superposition photon dose calculations for radiotherapy treatment planning *Phys. Med. Biol.* **48** 2873–93

Bedford J L, Child P J, Nordmark H V, Mosleh-Shirazi M A, Verhaegen F and Warrington A P 2003 Commissioning and quality assurance of the Pinnacle^3 radiotherapy treatment planning system for external beam photons *Br. J. Radiol.* **76** 163–76

Carrasco P, Jornet N, Duch M A, Weber L, Ginjaume M, Eudaldo T, Jurado D, Ruiz A and Ribas M 2004 Comparison of dose calculation algorithms in phantoms with lung equivalent heterogeneities under conditions of lateral electronic disequilibrium *Med. Phys.* **31** 2899–911

Dogan N, Siebers J V and Keall P J 2006 Clinical comparison of head and neck and prostate IMRT plans using absorbed dose to medium and absorbed dose to water *Phys. Med. Biol.* **51** 4967–80

Garcia-Vicente F, Minambres A, Jerez I, Modolell I and Torres J 2003 Experimental validation tests of fast Fourier transform convolution and multigrid superposition algorithms for dose calculation in low-density media *Radiother. Oncol.* **67** 239–49

IAEA TRS-430 2005 (Vienna: IAEA)

ICRU Report 44 1989 *Tissue Substitutes in Radiation Dosimetry and Measurement* (Oxford: Oxford University Press)

IEC62083 2000 *Medical Electrical Equipment—Requirements for the Safety of Radiotherapy Treatment Planning Systems* 1st edn (IEC62083) (Geneva: IEC)

Jones A O and Das I J 2005 Comparison of inhomogeneity correction algorithms in small photon fields *Med. Phys.* **32** 766–76

Kawrakow I 2000a Accurate condensed history Monte Carlo simulation of electron transport. I. EGSnrc, the new EGS4 version *Med. Phys.* **27** 485–98

Kawrakow I 2000b Accurate condensed history Monte Carlo simulation of electron transport: II. Application to ion chamber response simulations *Med. Phys.* **27** 499–513

Kawrakow I, Rogers D W and Walters B R 2004 Large efficiency improvements in BEAMnrc using directional bremsstrahlung splitting *Med. Phys.* **31** 2883–98

Knöös T, Ahnesjö A, Nilsson P and Weber L 1995 Limitations of a pencil-beam approach to photon dose calculations in lung tissue *Phys. Med. Biol.* **40** 1411–20

Knöös T, Ceberg C, Weber L and Nilsson P 1994 The dosimetric verification of a pencil-beam based treatment planning system *Phys. Med. Biol.* **39** 1609–28

Knöös T, Wieslander E, Cozzi L, Brink C, Fogliata A, Albers D, Nyström A and Lassen S 2006 Comparison of dose calculation algorithms for treatment planning in external photon beam therapy for clinical situations *Phys. Med. Biol.* **51** 5785–807

Krieger T and Sauer O A 2005 Monte Carlo- versus pencil-beam-/collapsed-cone-dose calculation in a heterogeneous multi-layer phantom *Phys. Med. Biol.* **50** 859–68

Low D, Harms W, Mutic S and Purdy J 1998 A technique for the quantitative evaluation of dose distributions *Med. Phys.* **25** 656–660

Mackie T R, Bielajew A F, Rogers D W O and Battista J J 1988 Generation of photon energy deposition kernels using the EGS Monte Carlo code *Phys. Med. Biol.* **33** 1–20

McNutt T R, Mackie T R, Reckwerdt P, Papanikolaou N and Paliwal B R 1996 Calculation of portal dose using the convolution/superposition method *Med. Phys.* **23** 527–35

Miften M, Wiesmeyer M, Kapur A and Ma C M 2001 Comparison of RTP dose distributions in heterogeneous phantoms with the BEAM Monte Carlo simulation system *J. Appl. Clin. Med. Phys.* **2** 21–31

Miften M, Wiesmeyer M, Monthofer S and Krippner K 2000 Implementation of FFT convolution and multigrid superposition models in the FOCUS RTP system *Phys. Med. Biol.* **45** 817–33

Mijnheer B, Olszewska A, Fiorino C, Hartmann G, Knöös T, Rosenwald J C and Welleweerd H 2004 (Brussels: ESTRO)

Nisbet A, Beange I, Vollmar H S, Irvine C, Morgan A and Thwaites D I 2004 Dosimetric verification of a commercial collapsed cone algorithm in simulated clinical situations *Radiother. Oncol.* **73** 79–88

Paelinck L, Reynaert N, Thierens H, De Neve W and De Wagter C 2005 Experimental verification of lung dose with radiochromic film: comparison with Monte Carlo simulations and commercially available treatment planning systems *Phys. Med. Biol.* **50** 2055–69

Papanikolaou N, Mackie T R, Meger-Wells C, Gehring M and Reckwerdt P 1993 Investigation of the convolution method for polyenergetic spectra *Med. Phys.* **20** 1327–36

Rogers D W, Faddegon B A, Ding G X, Ma C M, We J and Mackie T R 1995 BEAM: a Monte Carlo code to simulate radiotherapy treatment units *Med. Phys.* **22** 503–24

Siebers J V, Keall P J, Nahum A E and Mohan R 2000 Converting absorbed dose to medium to absorbed dose to water for Monte Carlo based photon beam dose calculations *Phys. Med. Biol.* **45** 983–95

Storchi P and Woudstra E 1996 Calculation of the absorbed dose distribution due to irregularly shaped photon beams using pencil-beam kernels derived form basic beam data *Phys. Med. Biol.* **41** 637–56

Storchi P R M, van Battum L J and Woudstra E 1999 Calculation of a pencil-beam kernel from measured photon beam data *Phys. Med. Biol.* **44** 2917–28

Ulmer W and Harder D 1995 A triple Gaussian pencil beam model for photon beam treatment planning *Z. Med. Phys.* **5** 25–30

Ulmer W and Harder D 1996 Applications of a triple Gaussian pencil beam model for photon beam treatment planning *Z. Med. Phys.* **6** 68–74

Ulmer W, Pyyry J and Kaissl W 2005 A 3D photon superposition/convolution algorithm and its foundation on results of Monte Carlo calculations *Phys. Med. Biol.* **50** 1767–90

Webb S and Fox R A 1980 Verification by Monte Carlo methods of a power law tissue-air ratio algorithm for inhomogeneity corrections in photon beam dose calculations *Phys. Med. Biol.* **25** 225–40

Weber L and Nilsson P 2002 Verification of dose calculations with a clinical treatment planning system based on a point kernel dose engine *J. Appl. Clin. Med. Phys.* **3** 73–87

Wieslander E and Knöös T 2000 A virtual linear accelerator for verification of treatment planning systems *Phys. Med. Biol.* **45** 2887–96

Wieslander E and Knöös T 2003 Dose perturbation in the presence of metallic implants: treatment planning system versus Monte Carlo simulations *Phys. Med. Biol.* **48** 3295–305